Analysis of Slotted, Dielectrically Loaded, Ridged Waveguide

ALFRED T. VILLENEUVE, SENIOR MEMBER, IEEE

Abstract—**This paper considers a symmetrical double-ridged waveguide with an axial dielectric slab inserted into it. Series expansions are used to describe the waveguide fields. The method of moments is employed to provide a system of linear equations from which the propagation constant and the coefficients of the series expansions are obtained. From these quantities, the field distributions and power flow are determined and a characteristic impedance based on a power–voltage definition is computed. The calculated propagation constants are compared with measured values.**

I. Introduction

THIS PAPER considers a symmetrical, double-ridged waveguide with an axial dielectric slab inserted into it. This slab is centered along the guide axis and it may have any width from zero up to the width of the slot in which it is located. Ridged waveguide is useful because, among other things, it permits wave propagation with smaller overall guide dimensions than would be required by rectangular guide. By introducing the dielectric slab, the propagation constant and characteristic impedance of the waveguide can be modified. Knowledge of the propagation constant and the characteristic impedance are necessary to design matched waveguide devices.

Ridged waveguide has been considered by various investigators over the past 30 to 40 years [1]–[9]. Most of these investigators use various approximate techniques that treat the ridge as a shunt susceptance; they apply a transverse resonance procedure to determine cutoff wavelengths. Several investigators have used modal expansions of the fields and mode-matching or integral equation techniques to determine the guide properties [6], [8], [9]. Only two authors appear to have considered the dielectric-slab loaded ridged waveguide [7]–[9]. Young used the transverse resonance technique to get an approximate solution for the propagation constants. His analysis seems to neglect the coupling of higher order TE and TM fields that is caused by the presence of the slab. However, he shows good agreement between calculated and measured values of the dominant-mode propagation constants. Magerl used a mode-matching technique to calculate propagation constants of a ridged guide whose ridge section was completely filled with dielectric. However, he incorrectly assumed, *a priori*, that the modes were TE and his results are only correct at cutoff [9].

All of the investigators but Mihran considered unslotted ridged guides. Mihran considered a slotted ridged guide without dielectric loading and used a combination of experimental capacitance measurements and a transverse resonance procedure to determine the cutoff wavelength, and subsequently, the characteristic impedance of the guide [2].

In this paper, the slotted, dielectrically loaded, ridged waveguide has been treated with a full modal solution which yields the propagation constant and characteristic impedance of the guide. The calculated values of the propagation constants are compared with measured values and excellent agreement is shown.

Manuscript received October 3, 1983; revised April 30, 1984.

The author is with the Antenna Department, Radar Systems Group, Hughes Aircraft Co., P.O. Box 92426, Bldg. R2, M/S A102, El Segundo, CA 90009.

II. Analysis

The waveguide configuration considered in this study is shown in Fig. 1. The modes of interest are the y-polarized modes, particularly the dominant mode. This analysis, however, applies to all even y-polarized modes. The guide is symmetrical; each half is divided into four regions that may each contain a different material. The central region approximates the slot if b_1 is made large enough to keep the positions of the top and bottom walls in the region from affecting the solution. The configuration is quite general; it allows for computations for a wide variety of guide/dielectric geometries.

A. Field Configuration

In general, the modes in the slab-loaded, ridged waveguide are neither TE nor TM to the guide axis. However, in each region they may be expressed as a superposition of parallel plate modes that are TE and TM to the x direction. In the ith region, the fields may be expressed as

$$\boldsymbol{E}^{(i)} = \boldsymbol{u}_x \sum_{n=2,4,\cdots} \frac{\left[\left(\frac{n\pi}{b_i}\right)^2 + k_z^2\right]}{j\omega\epsilon_i} I_n^{(i)}(x)\psi_n^{(i)} + \sum_{n=0,2,\cdots} \hat{V}_n^{(i)}(x)\hat{\boldsymbol{e}}_n^{(i)} + \sum_{n=2,4,\cdots} V_n^{(i)}(x)\boldsymbol{e}_n^{(i)} \quad (1a)$$

$$\boldsymbol{H}^{(i)} = \boldsymbol{u}_x \sum_{n=0,2,\cdots} \frac{\left[\left(\frac{n\pi}{b_i}\right)^2 + k_z^2\right]}{j\omega\mu_i} \hat{V}_n^{(i)}(x)\hat{\psi}_n^{(i)} + \sum_{n=0,2,\cdots} \hat{I}_n^{(i)}(x)\hat{\boldsymbol{h}}_n^{(i)} + \sum_{n=2,4,\cdots} I_n^{(i)}(x)\boldsymbol{h}_n^{(i)}. \quad (1b)$$

In (1a) and (1b), the symbols have the following meanings:

$$\hat{\psi}_n^{(i)} \equiv \sqrt{\frac{E_n}{b_i\left[\left(\frac{n\pi}{b_i}\right)^2 + k_z^2\right]}} \cos\left(\frac{n\pi}{b_i}y\right) e^{-jk_z z} \quad (2a)$$

0018-9480/84/1000-1302$01.00 ©1984 IEEE

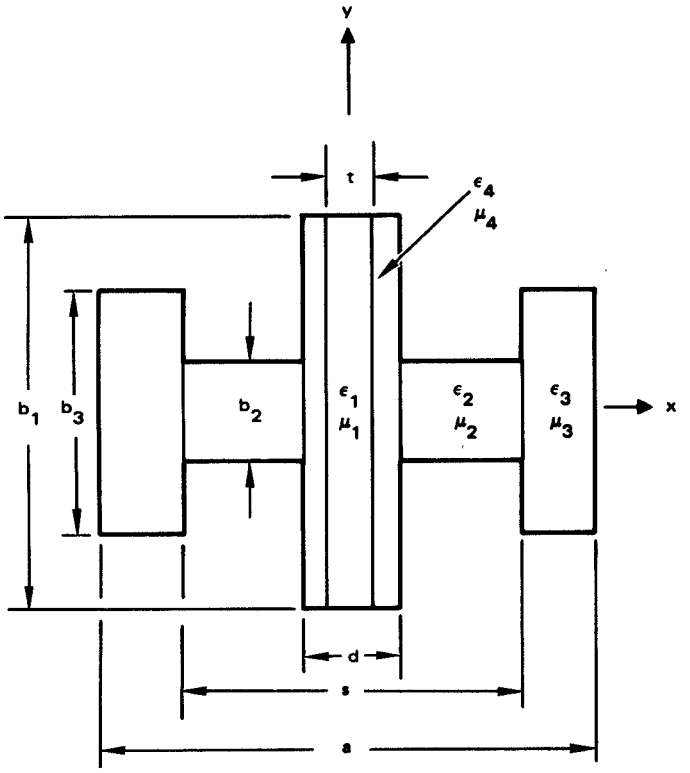

Fig. 1. Slotted, dielectrically loaded, ridged waveguide cross section.

$$\psi_n^{(i)} \equiv \sqrt{\frac{2}{b_i\left[\left(\frac{n\pi}{b_i}\right)^2 + k_z^2\right]}} \sin\left(\frac{n\pi y}{b_i}\right) e^{-jk_z z} \tag{2b}$$

$$\hat{e}_n^{(i)} \equiv u_x \times \nabla_t \hat{\psi}_n^{(i)} \tag{2c}$$

$$\hat{h}_n^{(i)} \equiv -\nabla_t \hat{\psi}_n^{(i)} = u_x \times \hat{e}_n^{(i)} \tag{2d}$$

$$e_n^{(i)} \equiv -\nabla_t \psi_n^{(i)} \tag{2e}$$

$$h_n^{(i)} \equiv -u_x \times \nabla_t \psi_n^{(i)} = u_x \times e^{(i)} \tag{2f}$$

$$\nabla_t = u_y \frac{\partial}{\partial y} + u_z \frac{\partial}{\partial z} \tag{2g}$$

where

k_z the propagation constant,
ϵ_i permittivity of ith region,
μ_i permeability of ith region,
b_i height of ith region,
E_n 1 if $n = 0$,
E_n 2 if $n > 0$.

Equations (1) and (2) are analogous to those of Harrington [10] except that they are formulated in terms of fields that are TE and TM to the x axis instead of to the z axis, and the mode functions are functions of y and z, rather than of x and y.

On using the expressions for $\hat{\psi}_n^{(i)}$ and $\psi_n^{(i)}$, the $\hat{e}_n^{(i)}$ and $e_n^{(i)}$ we have the following forms:

$$\hat{e}_n^{(i)} = \sqrt{\frac{E_n}{b_i\left[\left(\frac{n\pi}{b_i}\right)^2 + k_z^2\right]}} \left[u_y jk_z \cos\left(\frac{n\pi}{b_i} y\right) - u_z \left(\frac{n\pi}{b_i}\right) \sin\left(\frac{n\pi}{b_i} y\right)\right] e^{-jk_z z} \tag{3a}$$

$$e_n^{(i)} = \sqrt{\frac{2}{b_i\left[\left(\frac{n\pi}{b_i}\right)^2 + k_z^2\right]}} \left[-u_y \left(\frac{n\pi}{b_i}\right) \cos\left(\frac{n\pi}{b_i} y\right) + u_z jk_z \sin\left(\frac{n\pi y}{b_i}\right)\right] e^{-jk_z z}. \tag{3b}$$

Similarly, $\hat{h}_n^{(i)}$ and $h_n^{(i)}$ are given by the following expressions:

$$\hat{h}_n^{(i)} = \sqrt{\frac{E_n}{b_i\left[\left(\frac{n\pi}{b_i}\right)^2 + k_z^2\right]}} \left[u_y \left(\frac{n\pi}{b_i}\right) \sin\left(\frac{n\pi}{b_i} y\right) + u_z jk_z \cos\left(\frac{n\pi}{b_i} y\right)\right] e^{-jk_z z} \tag{4a}$$

$$h_n^{(i)} = \sqrt{\frac{2}{b_i\left[\left(\frac{n\pi}{b_i}\right)^2 + k_z^2\right]}} \left[-u_y jk_z \sin\left(\frac{n\pi}{b_i} y\right) - u_z \left(\frac{n\pi}{b_i}\right) \cos\left(\frac{n\pi}{b_i} y\right)\right] e^{-jk_z z}. \tag{4b}$$

If a set of vector-mode functions $\tilde{e}_n^{(i)}$, $\tilde{\hat{h}}_n^{(i)}$, $\tilde{e}_n^{(i)}$, and $\tilde{h}_n^{(i)}$ are defined by replacing k_z with $-k_z$ in (3) and (4), the following integral relationships are satisfied:

$$\int_{-b_i/2}^{b_i/2} e_n^{(i)} \cdot \tilde{e}_m^{(i)}\, dy = \int_{-b_i/2}^{b_i/2} h_n^{(i)} \cdot \tilde{h}_m^{(i)}\, dy = \delta_{nm} \tag{5a}$$

$$\int_{-b_i/2}^{b_i/2} \hat{e}_n^{(i)} \cdot \tilde{\hat{e}}_m^{(i)}\, dy = \int_{-b_i/2}^{b_i/2} \hat{h}_n^{(i)} \cdot \tilde{\hat{h}}_m^{(i)}\, dy = \delta_{nm} \tag{5b}$$

$$\int_{-b_i/2}^{b_i/2} \hat{e}_n^{(i)} \cdot \tilde{e}_m^{(i)}\, dy = \int_{-b_i/2}^{b_i/2} \hat{h}_n^{(i)} \cdot \tilde{h}_m^{(i)}\, dy = 0 \tag{5c}$$

where δ_{nm} is the Kronecker delta ($=1$ if $m = n$; $=0$ if $m \neq n$). In the lossless case, k_z is purely real for propagating modes and, from the definitions of the tilded-mode functions and from (3) and (4), it is evident that when no loss is present, the tilded-mode functions are complex conjugates of those in (3) and (4).

The $I_n(x)$'s and $V_n(x)$'s represent the modal currents and voltages, respectively. They are appropriate solutions of the one-dimensional wave equation

$$\frac{d^2 u_n^{(i)}}{dx^2} + k_{x\,\mathrm{in}}^2 u_n^{(i)} = 0 \tag{6}$$

where

$$k_{x\,\mathrm{in}}^2 = \omega^2 \mu_i \epsilon_i - \left(\frac{n\pi}{b_i}\right)^2 - k_z^2. \tag{7}$$

They also satisfy the following conditions:

$$\hat{I}_n^{(i)} = -\frac{1}{j\omega\mu_i} \frac{d\hat{V}_n^{(i)}}{dx} \tag{8a}$$

$$V_n^{(i)} = -\frac{1}{j\omega\epsilon_i} \frac{dI_n^{(i)}}{dx}. \tag{8b}$$

The fields in each region can be expressed with the above equations.

In the field expressions, the propagation constant k_z is the unknown quantity. To find this unknown, the analysis

uses the method of moments at the boundaries to get a set of homogeneous simultaneous linear equations for the V_ns and the I_ns. The propagation constant is the value of k_z for which the determinant of the system vanishes. With this value, the corresponding eigenvector of the determinant is computed and the values of V_n and I_n in each region are determined. With these quantities determined, the fields and corresponding power flow are computed and the characteristic impedance is calculated. The procedure is described in the following sections.

B. Derivation of Equations

The expressions for the voltages and currents in the various regions are considered first. In region 1, the voltage distribution is taken to be symmetrical in x and the expressions may be written as follows:

$$\hat{V}_n^{(1)} = \hat{C}_n^{(1)} \cos(k_{x1n} x) \tag{9a}$$

$$\hat{I}_n^{(1)} = \frac{k_{x1n}}{j\omega\mu_1} \hat{C}_n^{(1)} \sin(k_{x1n} x) \tag{9b}$$

$$V_n^{(1)} = -\frac{k_{x1n}}{j\omega\epsilon_1} C_n^{(1)} \cos(k_{x1n} x) \tag{9c}$$

$$I_n^{(1)} = C_n^{(1)} \sin(k_{x1n} x). \tag{9d}$$

In region 2, the voltages and currents consist of waves traveling or attenuating in both directions as follows:

$$\hat{V}_n^{(2)} = \hat{A}_n^{(2)} e^{-jk_{x2n}(x-d/2)} + \hat{B}_n^{(2)} e^{jk_{x2n}(x-s/2)} \tag{10a}$$

$$\hat{I}_n^{(2)} = \frac{k_{x2n}}{\omega\mu_2}\left[\hat{A}_n^{(2)} e^{-jk_{x2n}(x-d/2)} - \hat{B}_n^{(2)} e^{jk_{x2n}(x-s/2)}\right] \tag{10b}$$

$$V_n^{(2)} = A_n^{(2)} e^{-jk_{x2n}(x-d/2)} + B_n^{(2)} e^{jk_{x2n}(x-s/2)} \tag{10c}$$

$$I_n^{(2)} = \frac{\omega\epsilon_2}{k_{x2n}}\left[A_n^{(2)} e^{-jk_{x2n}(x-d/2)} - B_n^{(2)} e^{jk_{x2n}(x-s/2)}\right. . \tag{10d}$$

In region 3, the voltages and currents are standing waves with a vanishing voltage at the wall ($x = a/2$). They are represented by the following equations:

$$\hat{V}_n^{(3)} = \hat{C}_n^{(3)} \sin\left(k_{x3n}\left[\frac{a}{2} - x\right]\right) \tag{11a}$$

$$\hat{I}_n^{(3)} = \frac{k_{x3n}}{j\omega\mu_3} \hat{C}_n^{(3)} \cos\left(k_{x3n}\left[\frac{a}{2} - x\right]\right) \tag{11b}$$

$$V_n^{(3)} = -\frac{k_{x3n}}{j\omega\epsilon_3} C_n^{(3)} \sin\left(k_{x3n}\left[\frac{a}{2} - x\right]\right) \tag{11c}$$

$$I_n^{(3)} = C_n^{(3)} \cos\left(k_{x3n}\left[\frac{a}{2} - x\right]\right). \tag{11d}$$

Finally, in region 4, the voltages and currents are waves traveling or attenuating in both directions as follows:

$$\hat{V}_n^{(4)} = \hat{A}_n^{(4)} e^{-jk_{x4n}(x-t/2)} + \hat{B}_n^{(4)} e^{jk_{x4n}(x-d/2)} \tag{12a}$$

$$\hat{I}_n^{(4)} = \frac{k_{x4n}}{\omega\mu_4}\left[\hat{A}_n^{(4)} e^{-jk_{x4n}(x-t/2)} - \hat{B}_n^{(4)} e^{jk_{x4n}(x-d/2)}\right] \tag{12b}$$

$$V_n^{(4)} = A_n^{(4)} e^{-jk_{x4n}(x-t/2)} + B_n^{(4)} e^{jk_{x4n}(x-d/2)} \tag{12c}$$

$$I_n^{(4)} = \frac{\omega\epsilon_4}{k_{x4n}}\left[A_n^{(4)} e^{-jk_{x4n}(x-t/2)} - B_n^{(4)} e^{jk_{x4n}(x-d/2)}\right]. \tag{12d}$$

C. Application of Boundary Conditions

The requirement of continuity of the components of E and H parallel to the interface x_{ij} between region i and region j, results in the following pair of equations:

$$\sum_{n=0,2,\cdots} \hat{V}_n^{(i)}(x_{ij})\hat{\boldsymbol{e}}_n^{(i)} + \sum_{n=2,4,\cdots} V_n^{(i)}(x_{ij})\boldsymbol{e}_n^{(i)} = \sum_{n=0,2,\cdots} \hat{V}_n^{(j)}(x_{ij})\hat{\boldsymbol{e}}_n^{(j)} + \sum_{n=2,4,\cdots} V_n^{(1)}(x_{ij})\boldsymbol{e}_n^{(j)} \tag{13a}$$

$$\sum_{n=0,2,\cdots} \hat{I}_n^{(i)}(x_{ij})\hat{\boldsymbol{h}}_n^{(i)} + \sum_{n=2,4,\cdots} I_n^{(i)}(x_{ij})\boldsymbol{h}_n^{(i)} = \sum_{n=0,2,\cdots} \hat{I}_n^{(j)}(x_{ij})\hat{\boldsymbol{h}}_n^{(j)} + \sum_{n=2,4,\cdots} I_n^{(j)}(x_{ij})\boldsymbol{h}_n^{(j)}. \tag{13b}$$

These equations may be reduced to a set of simultaneous linear equations by multiplying (13a) successively by $\tilde{\hat{\boldsymbol{e}}}_m^{(i)}$ and by $\tilde{\boldsymbol{e}}_m^{(i)}$ where $b_i \geqslant b_j$ and integrating the resulting expressions over y. Because the tangential electric field on the i side of the junction vanishes for $|y| > b_j/2$, the integral on that side may be extended to $b_i/2$ with the following result:

$$\hat{V}_m^{(i)}(x_{ij}) = \sum_{n=0,2,\cdots} \hat{V}_n^{(j)} \mathcal{J}_{\hat{m}\hat{n}}^{(ij)} + \sum_{n=2,4,\cdots} V_n^{(j)} \mathcal{J}_{\hat{m}n}^{(ij)}, \quad \hat{m} = 0,2,\cdots \tag{14a}$$

$$V_m^{(i)}(x_{ij}) = \sum_{n=0,2,\cdots} \hat{V}_n^{(j)} \mathcal{J}_{m\hat{n}}^{(ij)} + \sum_{n=2,4,\cdots} V_n^{(j)} \mathcal{J}_{mn}^{(ij)}, \quad m = 2,4,\cdots \tag{14b}$$

where

$$\mathcal{J}_{\hat{m}\hat{n}}^{(ij)} \equiv \int_{-b_j/2}^{b_j/2} \tilde{\hat{\boldsymbol{e}}}_m^{(i)} \cdot \hat{\boldsymbol{e}}_n^{(j)}\, dy \tag{15a}$$

$$\mathcal{J}_{\hat{m}n}^{(ij)} \equiv \int_{-b_j/2}^{b_j/2} \tilde{\hat{\boldsymbol{e}}}_m^{(i)} \cdot \boldsymbol{e}_n^{(j)}\, dy \tag{15b}$$

$$\mathcal{J}_{m\hat{n}}^{(ij)} \equiv \int_{-b_j/2}^{b_j/2} \tilde{\boldsymbol{e}}_m^{(i)} \cdot \hat{\boldsymbol{e}}_n^{(j)}\, dy \tag{15c}$$

$$\mathcal{J}_{mn}^{(ij)} \equiv \int_{-b_j/2}^{b_j/2} \tilde{\boldsymbol{e}}_m^{(i)} \cdot \boldsymbol{e}_n^{(j)}\, dy. \tag{15d}$$

The integrals on the j side extend only over $b_j/2$ because the j-mode functions to not extend beyond those limits. After multiplying (13b) successively by $\hat{\boldsymbol{h}}_m^{(j)}$ and $\tilde{\boldsymbol{h}}_m^{(j)}$ and integrating it over y from $-b_j/2$ to $+b_j/2$, the following sets of equations result:

$$\hat{I}_m^{(j)} = \sum_{n=0,2,\cdots} \hat{I}_n^{(i)} \mathcal{J}_{\hat{m}\hat{n}}^{(ji)} + \sum_{n=2,4,\cdots} I_n^{(i)} \mathcal{J}_{\hat{m}n}^{(ji)} \tag{16a}$$

$$I_m^{(j)} = \sum_{n=0,2,\cdots} \hat{I}_n^{(i)} \mathcal{J}_{m\hat{n}}^{(ji)} + \sum_{n=2,4,\cdots} I_n^{(i)} \mathcal{J}_{mn}^{(ji)} \tag{16b}$$

where

$$\mathcal{J}_{\hat{m}\hat{n}}^{(ji)} \equiv \int_{-b_j/2}^{b_j/2} \tilde{\hat{\boldsymbol{h}}}_m^{(j)} \cdot \hat{\boldsymbol{h}}_n^{(i)}\, dy \tag{17a}$$

$$\mathcal{J}_{\hat{m}n}^{(ji)} \equiv \int_{-b_j/2}^{b_j/2} \tilde{\hat{\boldsymbol{h}}}_m^{(j)} \cdot \boldsymbol{h}_n^{(i)}\, dy \tag{17b}$$

$$\mathcal{J}_{m\hat{n}}^{(ji)} \equiv \int_{-b_j/2}^{b_j/2} \tilde{\boldsymbol{h}}_m^{(j)} \cdot \hat{\boldsymbol{h}}_n^{(i)}\, dy \tag{17c}$$

$$\mathcal{J}_{mn}^{(ji)} \equiv \int_{-b_j/2}^{b_j/2} \tilde{\boldsymbol{h}}_m^{(j)} \cdot \boldsymbol{h}_n^{(i)}\, dy. \tag{17d}$$

In view of the definitions of the $\boldsymbol{e}$ and $\boldsymbol{h}$ functions, it may be shown that

$$\mathcal{J}_{\hat{m}\hat{n}}^{(ji)} = \tilde{\mathcal{J}}_{\hat{n}\hat{m}}^{(ij)} \tag{18a}$$

$$\mathcal{J}_{\hat{m}n}^{(ji)} = \tilde{\mathcal{J}}_{n\hat{m}}^{(ij)} \tag{18b}$$

$$\mathcal{J}_{m\hat{n}}^{(ji)} = \tilde{\mathcal{J}}_{\hat{n}m}^{(ij)} \tag{18c}$$

$$\mathcal{J}_{mn}^{(ji)} = \tilde{\mathcal{J}}_{nm}^{(ij)} \tag{18d}$$

where the tilde over the $\mathcal{J}$'s indicates that the $\mathcal{J}$'s are evaluated with k_z replaced by $-k_z$. In the lossless case, the $\tilde{\mathcal{J}}$'s are the complex conjugates of the $\mathcal{J}$'s.

With (13)–(18) and (9)–(12), the systems can be truncated and solved for eigenvalues and eigenvectors. In the truncation, the number of modes used in each region must be sufficient to achieve the accuracy desired. Different numbers of terms will be required in each region of a different height. According to Lee *et al.*, the number of modes in a given region should be proportional to the height of that region relative to the smallest height [11]. Thus, the smallest number of modes would be required in the region of least height.

If the number of regions is not too large, the order of the system of equations to be solved may be reduced conveniently to the number of modes in the region of smallest height. This reduction may be accomplished by direct solution for the voltage and current coefficients of all other regions in terms of the coefficients in the region of smallest height. This procedure was carried out to obtain the system determinant. The details are quite involved and the resulting expressions are very complicated and for that reason are not included here.

D. Solution for the Propagation Constant

Let H denote the matrix of the coefficients. The propagation constants are those values of k_z that satisfy the following equation:

$$\det(H) = 0. \tag{19}$$

The required order of the determinant used in the calculations is determined by the accuracy required in the computed results.

The number of real roots (for the lossless case) is determined by the number of propagating modes at a given frequency. In the calculations that were performed, only the dominant mode was considered. The equations were programmed for the lossless case and the root was found using essentially the same technique as Montgomery [6].

E. Determination of Fields

When the eigenvalue k_z of the matrix H has been determined, the corresponding eigenvector may be obtained. The method used is the same as that used by Montegomery and is not described here. Once the $A^{(2)}$'s and $B^{(2)}$'s are determined, the coefficients of the fields in various other regions can be determined. With these coefficients, the field may be approximated at any point in the guide cross section. These fields were used in the calculations of the power flow along the guide as discussed in the following section.

F. Power Flow

The average power transmitted along the guide may be computed by integrating the longitudinal component of the Poynting vector over the guide cross section

$$P = \frac{1}{2}\int\int_{\text{AREA}} (\boldsymbol{E} \times \boldsymbol{H}^*) \cdot \boldsymbol{u}_z\, dx\, dy. \tag{20}$$

On using (1) and (3) in (20), the following expression for P_i, the power flow in the ith region, is obtained:

$$\begin{aligned} P_i = &\sum_{n=2,4,\cdots} \frac{1}{j\omega\epsilon_i}\left[\left(\frac{n\pi}{b_i}\right)\int_{x_{i1}}^{x_{i2}} I_n^{(i)} \hat{I}_n^{(i)*}\, dx \right. \\ &\left. + jk_z \int_{x_{i1}}^{x_{i2}} I_n^{(i)} I_n^{(i)*}\, dx\right] \\ &+ \sum_{n=0,2,\cdots} \frac{k_z}{\omega\mu_i}\int_{x_{i1}}^{x_{i2}} \hat{V}_n^{(i)} \hat{V}_n^{(i)*}\, dx \\ &- \sum_{n=2,4,\cdots} \frac{1}{j\omega\mu_i}\left(\frac{n\pi}{b_i}\right)\int_{x_{i1}}^{x_{i2}} V_n^{(i)} \hat{V}_n^{(i)*}\, dx. \end{aligned} \tag{21}$$

The actual value of P_i is obtained by using the numerical values of the modal coefficients in (21) along with their functional forms given in (9) through (12). The total power flow P_t is the sum of the power flow in each region.

G. Characteristic Impedance

In waveguide, the definition of characteristic impedance is not unique. One method that has been used to define characteristic impedance by a number of investigators [2], [3], [6] is based on the power transmitted along the guide and a "voltage," defined as the line integral of the electric-field strength along some path from the top to bottom walls. If this path is taken along the path $x = 0$, i.e., along the center of the cross section, the following equation results:

$$V_0 \equiv \int_{-b_1/2}^{b_1/2} E_y(0, y)\, dy = j\sqrt{b_1}\, \hat{C}_0^{(1)} e^{-jk_z z}. \tag{22}$$

The corresponding expression for characteristic impedance then becomes

$$Z_0 \equiv \frac{|V_0|^2}{2P_T} = \frac{b_1 |\hat{C}_0^{(1)}|^2}{2P_T}. \tag{23}$$

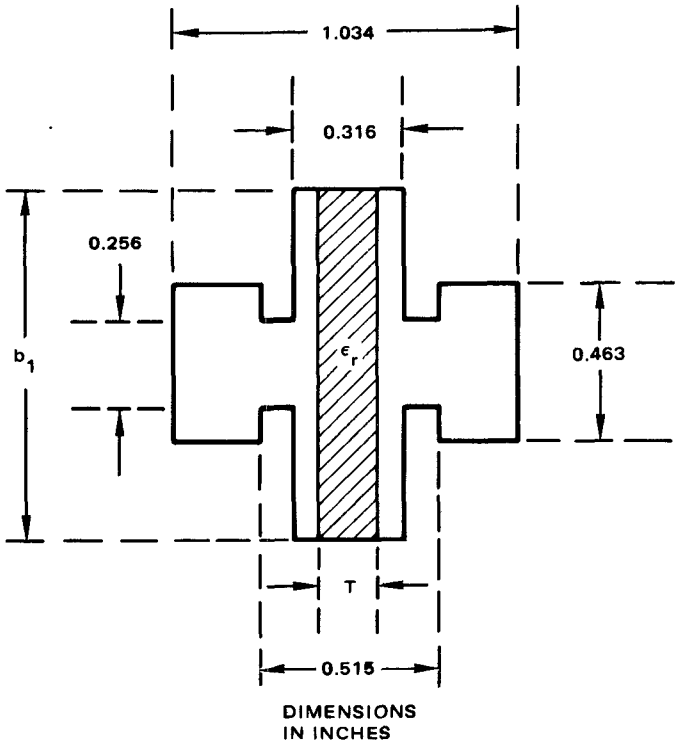

Fig. 2. Guide cross section for numerical analysis.

III. Numerical Results

A. Computer Programs

The equations for the propagation constant and for the characteristic impedance have been programmed for numerical calculations. They have been checked against available data for unloaded ridge guide calculations and the results agree [6].

B. Results for Slotted, Dielectric-Loaded Ridged Guide

Calculations were performed for the propagation constant and characteristic impedance of slotted, ridged waveguide with dielectric slabs of various widths along its axis. A typical cross section is shown in Fig. 2. The propagation constant and characteristic impedance change as the height of regions 1 and 4 increase from the value b_2. Fig. 3 illustrates that, beyond a certain height, the values of these quantities remain constant. Calculated values are given in Table I. All subsequent calculations on slotted guides were done for $b_1 = 1.056$ in because, beyond that value, the propagation constant and characteristic impedance are unaffected.

The effect of the slot in unloaded guide is shown in Fig. 4 and in Table II. It is evident that the presence of the slot may represent a large perturbation on the characteristics of the unslotted guide depending on the slot width. In Fig. 5, calculated values of the guide wavelengths and Z_0 are shown versus dielectric width. The calculated wavelengths are compared with measured values. The agreement is excellent; the differences are within experimental uncertainty. Table III shows the calculated results.

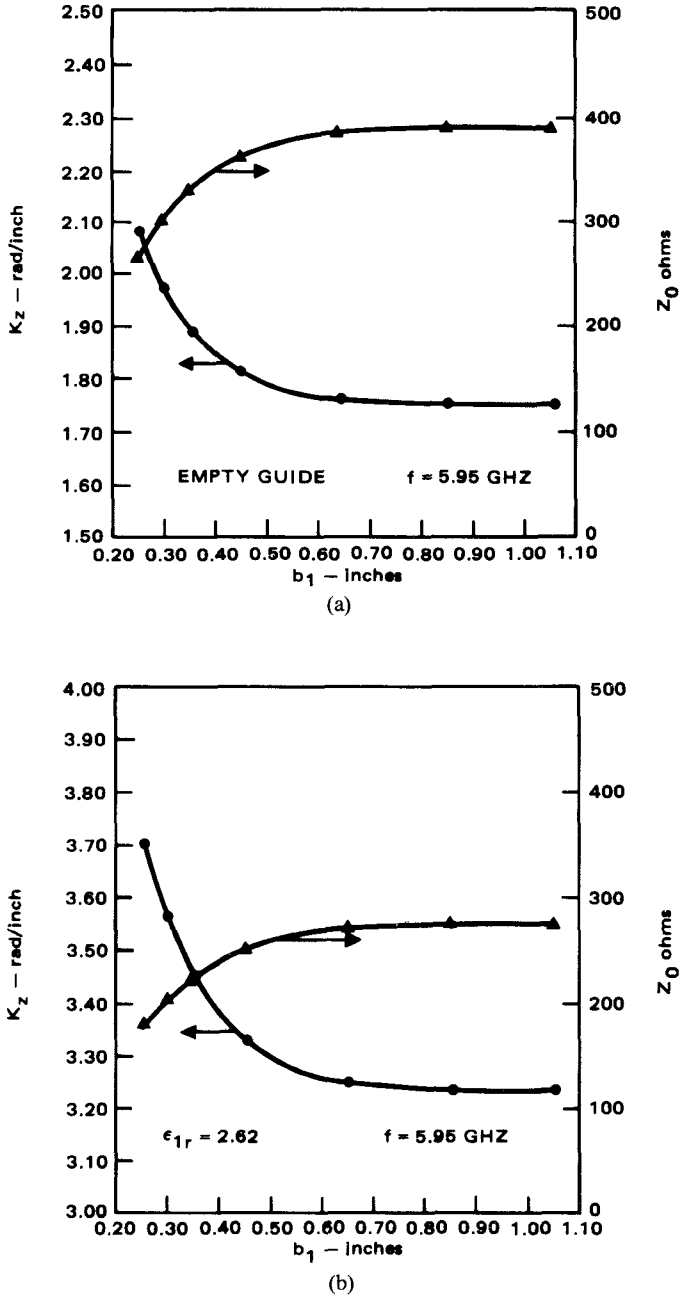

Fig. 3. Effect of slot depth on propagation constant and characteristic impedance.

TABLE I
Effect of Slot Height on Guide Parameters
(Slot Filled with Dielectric)
frequency = 5.95 GHz, slot width = 0.316 in

Slot Height b_1, in	ϵ_{1r} = 1 000			ϵ_{1r} = 2 62		
	k_z, rad/in	λ_g, in	Z_0, ohms	k_z, rad/in	λ_g, in	Z_0, ohms
0 256	2 07102	3 0339	265 16	3 69973	1 6983	177 83
0 300	1 96998	3 1895	300 77	3 56320	1 7634	202 83
0 350	1 89234	3 3203	330 40	3 45374	1 8192	224.47
0 450	1 80793	3 4753	365 32	3 32932	1 8872	251.50
0 650	1 75947	3 5711	387 05	3 25222	1 9320	270 29
0 850	1 75207	3 5861	390 56	3 23914	1 9404	273 83
1 056	1 75095	3 5884	391.11	3 23691	1 9411	274 47

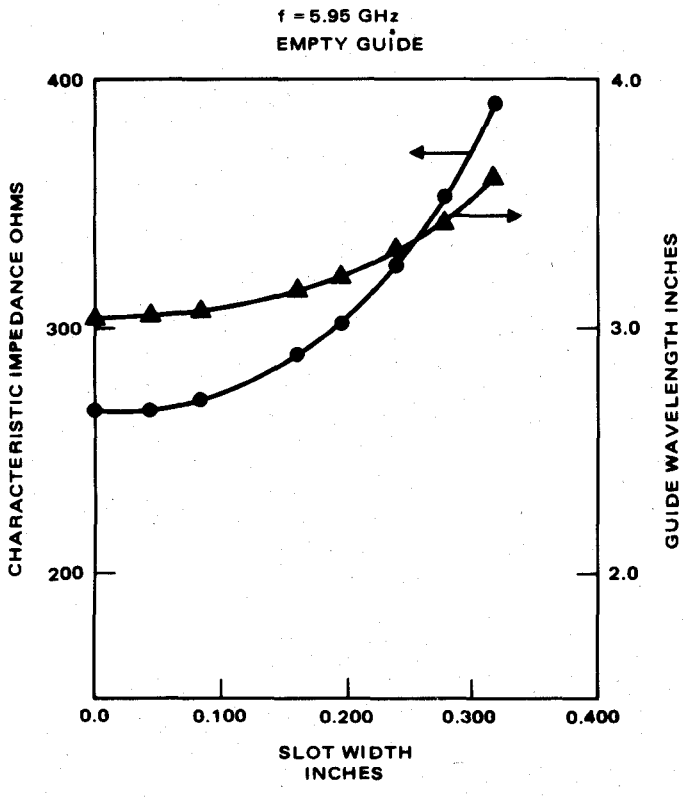

Fig. 4. Effect of slot width on unloaded guide.

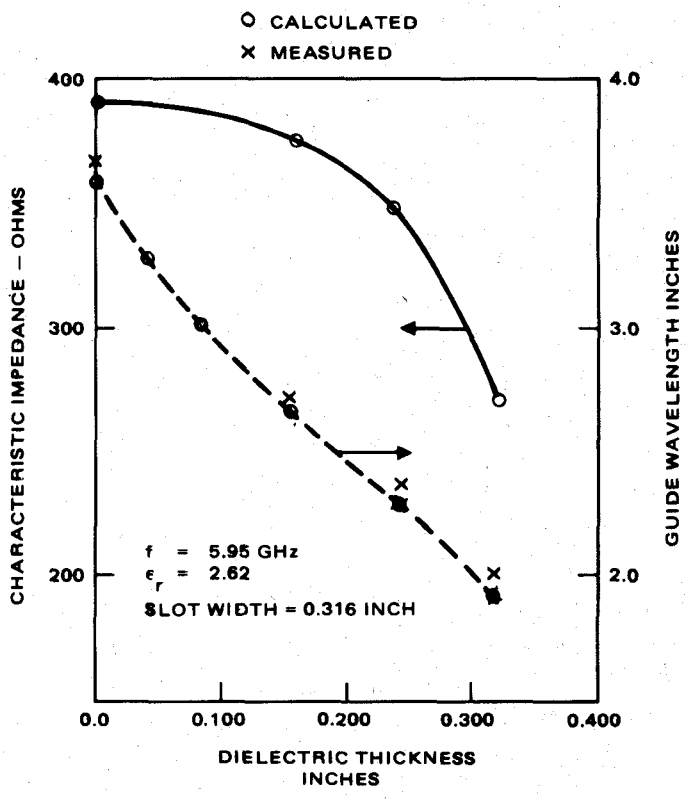

Fig. 5. Guide wavelength and characteristic impedance versus dielectric slab thickness.

TABLE II
EFFECT ON SLOT WIDTH D ON EMPTY GUIDE PARAMETERS
frequency = 5.95 GHz

Slot Width, d, in	k_z, rad/in	λ_g, in	Z_0, ohms
0.000	2.07102	3.0339	265.16
0.040	2.06604	3.0412	266.49
0.080	2.05119	3.0632	270.71
0.158	1.99378	3.1514	288.91
0.190	1.95912	3.2071	301.04
0.237	1.89571	3.3144	325.30
0.275	1.83259	3.4286	352.14
0.316	1.75095	3.5884	391.11

TABLE III
EFFECT OF DIELECTRIC THICKNESS ON SLOTTED GUIDE PARAMETERS
frequency = 5.95 GHz, slot width = 0.316 in, $\epsilon_{ir} = 2.62$

Dielectric Thickness, t, in	k_z, rad/in	λ_g, in	Z_0, ohms
0.000	1.75095	3.5884	391.11
0.040	1.91741	3.2769	388.57
0.080	2.07878	3.0225	385.67
0.158	2.37081	2.6502	374.95
0.237	2.70190	2.3225	342.57
0.316	3.23691	1.9411	274.47

C. Field Distributions

Calculated field distributions for the guide of Fig. 2 are shown in Figs. 6–10. Figs. 6, 9, and 10 show E_y, $-\eta_0 k/k_z H_x$, and $j\eta_0 k/k_z H_z$ versus x for $y = 0$ and for $y = 0.127$ in. Figs. 7 and 8 show all six field components for the same range in x and y. The value $y = 0$ corresponds to the central horizontal cut while the $y = 0.127$ in corresponds to a horizontal cut that passes just 0.001 in below the upper ridge. The curves of the transverse field components, E_y and H_x along the $y = 0$ line, show some slight irregularities as x passes directly beneath the sharp corners of the ridge. This effect is attributed to the convergence characteristics of their series representation, which must also approximate the necessary singularity of these fields as the sharp corners are approached, as illustrated in the cuts along $y = 0.127$. The actual fields along $y = 0$ should pass smoothly from one region to the next.[1] This irregularity does not occur for H_z because it is not singular at the ridge corners and the series representing it converges nicely everywhere.

Fig. 6(a) and (b) represents the case of the slotted guide with no dielectric, while Figs. 7(a) and (b) and 8(a) and (b) show the effect of inserting slabs of Rexolite 2200 ($\epsilon_r = 2.62$) into the slot. For all figures, in the plane $y = 0$, the field components E_z, E_x, and H_y vanish, but, as illustrated

[1]The use of additional terms in the series should improve the representation across the transition, but without significant improvement in overall results, and at the expense of additional computational costs. For all curves and Tables shown, the numbers of terms used in the computations were, in regions 1 and 4, 82 terms; in region 2, 20 terms; and in region 3, 36 terms. Use of as few as one-fourth as many terms does not significantly change the computed values of k_z and Z_0 but does markedly reduce computation time.

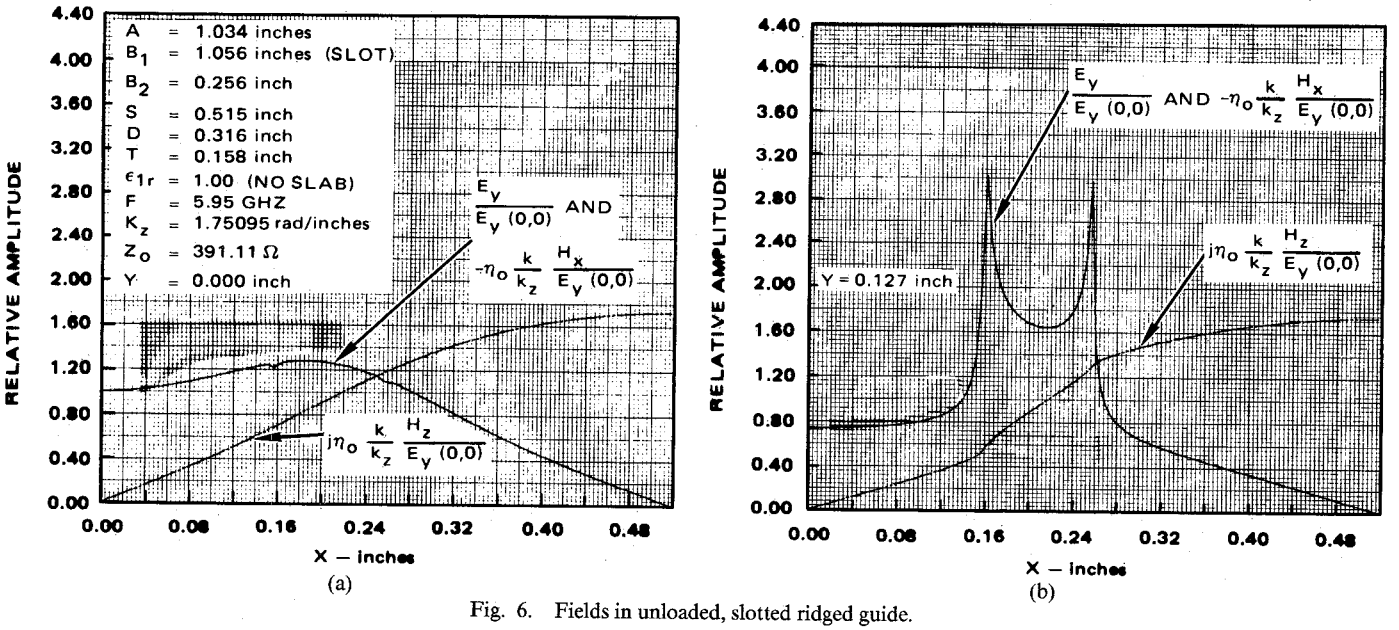

Fig. 6. Fields in unloaded, slotted ridged guide.

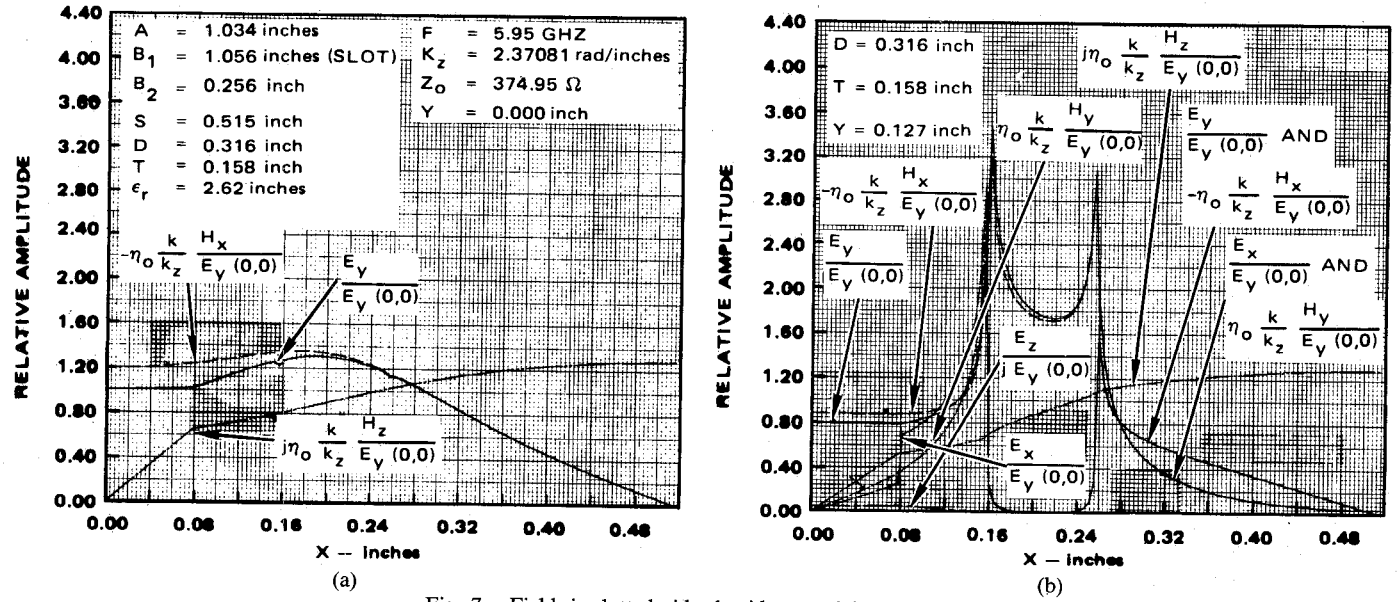

Fig. 7. Fields in slotted, ridged guide—partial slot loading.

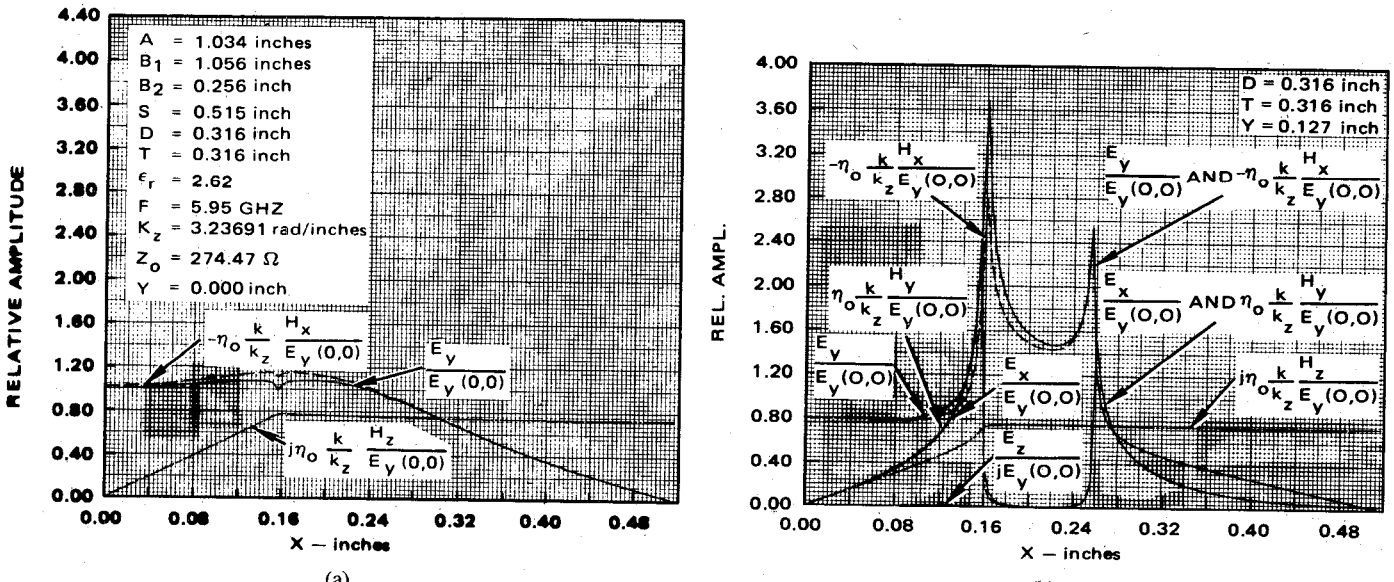

Fig. 8. Fields in slotted, ridged guide—full slot loading.

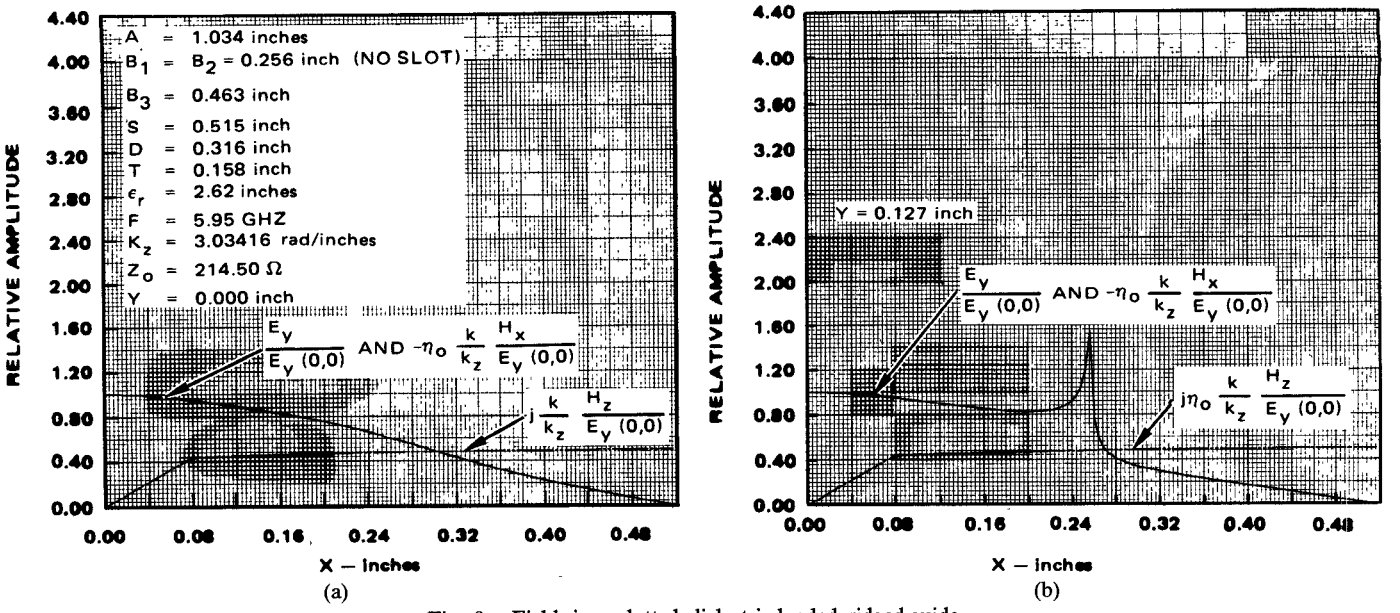

Fig. 9. Fields in unslotted, dielectric-loaded, ridged guide.

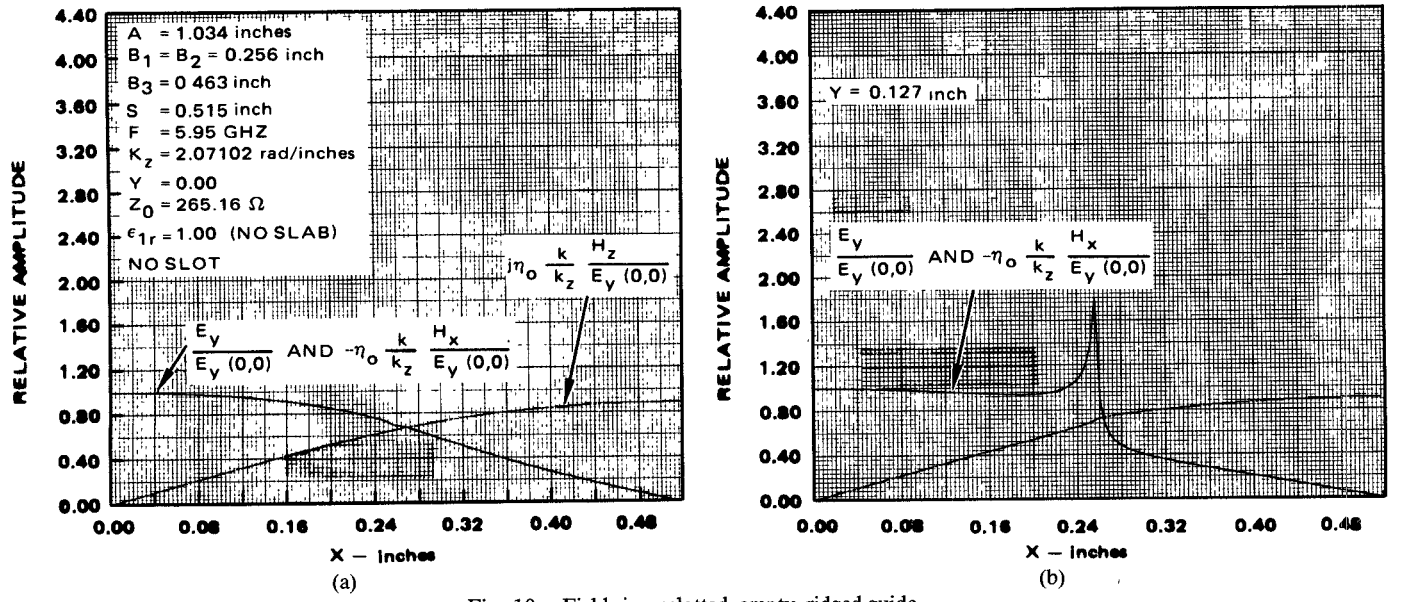

Fig. 10. Fields in unslotted, empty, ridged guide.

in Figs. 7(b) and 8(b), the presence of the ridges gives rise to an x component of E and a y component of H away from this plane. The presence of this dielectric, i.e., the inhomogeneity of the guide material, gives rise to the small z component of E. It is also evident that, when the dielectric is present in the ridged guide, E_y/H_x and E_x/H_y are not constant as they are in homogeneously filled guide. Thus, for the slab-loaded ridged guide there is no single wave impedance definable as in homogeneously filled guide.[2]

IV. Conclusions

A modal expansion method was applied to the analysis of the slotted, dielectrically loaded, ridged waveguide to permit calculation of the propagation constant, the characteristic impedance, and the field distributions of that configuration. These quantities are required in the design of matched waveguide devices.

Excellent agreement between calculated and measured propagation constants was obtained. The analysis is applicable to a wide variety of geometries and dielectric loadings and should prove useful in future work with ridged waveguide component design.

[2]In the special case of the dielectric slab-loaded rectangular waveguide, the TE_{n0} modes are TE to the z axis and there is a single wave impedance over the entire cross section.

Acknowledgment

Many thanks are due to T. Spehar and C. Williams who aided in the editing and preparation of this paper.

References

[1] S. B. Cohn, "Properties of ridge waveguide," *Proc. IRE*, vol. 35, no. 8, pp. 783–788, Aug. 1947.
[2] T. G. Mihran, "Closed- and open-ridge waveguide," *Proc. IRE*, vol. 37, no. 6, pp. 640–644, June 1949.
[3] S. Hopfer, "The design of ridged waveguides," *IRE Trans. Microwave Theory Tech.*, vol. MTT-3, pp. 20–29, Oct. 1955.

[4] T. S. Chen, "Calculations of the parameters of ridge waveguides," *IRE Trans. Microwave Theory Tech.*, vol. MTT-5, pp. 12–17, Jan. 1957.
[5] J. R. Pyle, "The cutoff wavelength of the TE_{10} mode in ridged rectangular waveguide of any aspect ratio," *IEEE Trans. Microwave Theory Tech.*, vol. MTT-14, pp. 175–183, Apr. 1966.
[6] J. P. Montgomery, "On the complete eigenvalue solution of ridged waveguide," *IEEE Trans. Microwave Theory Tech.*, vol. MTT-19, pp. 547–555, June 1971.
[7] W. C. Young, Jr., "TE-mode solutions for dielectric slab center-loaded ridged waveguide," NRL Rep. 8105, Apr. 29, 1977.
[8] G. Magerl, "Ridged waveguides with inhomogeneous dielectric slab loading," *IEEE Trans. Microwave Theory Tech.*, vol. MTT-26, pp. 413–416, June 1978.
[9] C. W. Young and G. Magerl, "Comments on ridged waveguides with inhomogeneous dielectric slab loading," *IEEE Trans. Microwave Theory Tech.*, vol. MTT-26, pp. 919, Nov. 1978.
[10] R. F. Harrington, *Time-Harmonic Electromagnetic Fields*. New York: McGraw-Hill, 1961, pp. 381–388.
[11] S. W. Lee, W. R. Jones, and J. J. Campbell, "Convergence of numerical solutions of iris-type discontinuity problems," *IEEE Trans. Microwave Theory Tech.*, vol. MTT-19, pp. 528–536, June 1971.

✤

Alfred T. Villeneuve (S'52–A'53–M'58–SM'82) was born in Syracuse, NY. He received the B.E.E. degree from Manhattan College, Bronx, NY, in 1952, and the M.E.E. and Ph.D. degrees from Syracuse University, Syracuse, NY, in 1955 and 1959, respectively.

From 1952 to 1955, he was a Research Associate in Electrical Engineering at Syracuse University, where he worked on UHF antennas and microwave filters. From 1956 to 1959, he was an Instructor in Electrical Engineering, teaching courses in electromagnetism and network theory. In 1959, he was promoted to Assistant Professor. In the same year, he joined Hughes Aircraft Co., where he is currently a Senior Scientist in the Antenna Department of the Radar Systems Group. He has been engaged in various aspects of antenna theory and design there over the past 25 years. He has been a lecturer at the University of Southern California, the University of California at Los Angeles, and at Loyola-Marymount University in Los Angeles.

Dr. Villeneuve has served as a reviewer for the IEEE TRANSACTIONS ON MICROWAVE THEORY AND TECHNIQUES and IEEE TRANSACTIONS ON ANTENNAS AND PROPAGATION and has served a term on the Administrative Committee of the Antennas and Propagation Society (AP-S). He also served as Secretary-Treasurer, Vice Chairman, and Chairman of the Los Angeles Chapter of AP-S. He is a member of the IEEE Antenna Standards Committee and was a member of Subcommittee 2.11 on Methods of Testing Antennas which recently published IEEE Std 149-1979, *IEEE Standard Test Procedures* for *Antennas*. He was a member of the Working Group on Definition of Terms for Antennas which recently completed IEEE Std 145-1983, *IEEE Standard Definitions of Terms for Antennas*. He served on the Steering Committees of the 1971 and 1981 International Antennas and Propagation Symposia and has also been on the Technical Program committees of these and several other symposia. He is a member of Eta Kappa Nu, Sigma Xi, and Commission B of the International Union of Radio Science.

Stability of Multifrequency Negative-Resistance Oscillators

BEVAN D. BATES, MEMBER, IEEE, AND PETER J. KHAN, SENIOR MEMBER, IEEE

Abstract—**A general criterion is derived for the stability of a negative-resistance oscillator with respect to small perturbations in the operating point. The derivation applies when the oscillator output consists of an arbitrary number of related frequency components, including possible nonharmonic components. Examples are given of the application of the stability criterion to coaxial IMPATT oscillator circuits, with experimental verification of the frequency and output power at theoretically determined stable operating points.**

I. INTRODUCTION

NEGATIVE-RESISTANCE devices find widespread application in microwave oscillators. As a consequence of the nonlinearity of the negative resistance and of the complicated frequency dependence of the impedance characteristic of the passive microwave circuit to which the device is connected, the resulting signal will generally contain harmonic components of the fundamental oscillation frequency. However, in the more general case, the frequency components in the oscillation may not be harmonically related due to parametric effects, and its up-converted low-frequency oscillation.

This paper presents expressions which permit determination of the stability of the oscillation state for the case where the device impedance is a function of both excitation and frequency, and an arbitrary number of frequency components are present. Use of the stability criteria derived here provides a more accurate determination of the oscillation characteristics of IMPATT and transferred-electron-device circuits using a realistic circuit model of the microwave mounting and impedance-transforming structure.

The oscillator stability studies derive from the fundamental work of Kurokawa [1], who developed a first-order theory describing the behavior of a one-port negative resistance embedded in a general passive multiple-resonant

Manuscript received October 24, 1983; revised May 17, 1984. Part of this work was performed at the Jet Propulsion Laboratory, California Institute of Technology, Pasadena, and was supported by the National Research Council under an agreement with the National Aeronautics and Space Administration.

B. D. Bates was a NRC-NASA Resident Research Associate, Jet Propulsion Laboratory, 4800 Oak Grove Drive, Pasadena, CA 91109. He is now with the Department of Electrical and Electronic Engineering, University of Melbourne, Victoria 3052, Australia.

P. J. Khan was with the Electrical Engineering Department, University of Queensland, St. Lucia, Queensland 4067, Australia. He is now with the Bahá'í World Centre, P.O. Box 155, Haifa, 31-001, Israel.

0018-9480/84/1000-1310$01.00 ©1984 IEEE